

# Coupled Electrorotation: Two Proximate Microspheres Spin in Registry with an AC Electric Field

Garth J. Simpson,<sup>\*[a]</sup> Clyde F. Wilson,<sup>[b]</sup> Karl-Heinz Gericke,<sup>[c]</sup> and Richard N. Zare<sup>\*[b]</sup>

We report a novel approach to micro- and nanoparticle rotation, uniting the fine translational control afforded by optical trapping with the flexibility and simplicity of dipole–field-induced coupled electrorotation (CER). Fluorescence imaging using a microparticle photopatterning technique was combined with optical trapping to quantify both the senses and speeds of rotation for individual pairs of particles. Laser tweezers allowed controlled positioning of a pair of particles within a dipole field while simultaneously providing an axis about which the particles rotated. The particle–particle interactions inherent in CER offer several distinct advantages compared with electrorotation in multipole fields. Results from

several investigations highlight the utility of this approach, including quantification of rotation in spheres as small as 750 nm in diameter, observation of rotation rates as high as 1800 rpm, fabrication of coupled electrorotational “antigears”, trapping and rotation of sphere dimers, and exploitation of the registry of sphere rotation to probe the dielectric properties of immobile objects.

## KEYWORDS:

electrorotation · fluorescence · nanostructures · photopatterning

## Introduction

With the rapid expansion of studies utilizing microfluidic total analysis systems (“labs on chips”) and microelectromechanical systems (MEMS), interest is growing in the generation of noncontact methods to manipulate microscopic and nanoscopic particles.<sup>[1, 2]</sup> Several well established approaches are available for microparticle translational manipulation (for example optical trapping,<sup>[3–5]</sup> electrophoresis,<sup>[6, 7]</sup> and dielectrophoresis<sup>[2, 6, 8, 9]</sup>). More recently, several ingenious approaches have been developed to control rotational motion of microscale and nanoscale particles, including a number of purely optical methods.<sup>[10–18]</sup> Several groups have demonstrated that radiation pressure can induce rotation in anisotropic particles through an optical “windmill” effect.<sup>[10–13]</sup> Microfabrication of the particle structure has allowed for rational control over the direction of rotation in these devices.<sup>[11, 12]</sup> Radiation pressure-driven rotation rates of 420 rpm have been experimentally observed for microfabricated particles,<sup>[10]</sup> and rates of up to 2200 rpm have been reported for ground glass powder particles.<sup>[13]</sup> Optical trapping of birefringent particles using circularly polarized light has also been demonstrated as a means to transfer angular momentum from the optical trap beam to an immobilized particle (in this case, photon spin angular momentum).<sup>[14, 15]</sup> Friese et al.<sup>[14]</sup> have demonstrated rotation rates for birefringent calcite particles in excess of 350 Hz (21 000 rpm) and shown that these particles can be used to drive rotation in optically trapped microfabricated particles at rates of  $\sim 0.2$  Hz.<sup>[15]</sup> Utilizing Laguerre–Gaussian (LG) modes in optical trap beams, Simpson et al.<sup>[16, 17]</sup> have induced rotation in partially absorbing particles by transfer of a combination of spin and/or orbital photon angular momentum. Recently, Paterson et al.<sup>[18]</sup> have demonstrated optical trapping within the interference pattern of an LG beam and a plane-


polarized beam as a means to either rotate rodlike particles or to revolve two or three particles about a central axis.

Despite the advantages of purely optical, noncontact techniques in inducing rotational motion in particles, potential limitations of several of these techniques are related to the somewhat stringent requirements on the particle shape and/or optical properties. For example, the highest rotation rates have been achieved for particles prepared through physical grinding of bulk samples into powders.<sup>[13, 14]</sup> Although simple, this manufacturing approach does not provide much flexibility for rational design. Additionally, the most widely used microfabrication techniques are not amenable to the generation of birefringent particles, which limits the range of methods with this requirement.<sup>[14, 15]</sup> In the optical “windmill” methods,<sup>[10–13]</sup> the shape of the microparticle was prepared such that the particle could be both optically trapped and made to rotate by the same

[a] Prof. G. J. Simpson  
Department of Chemistry  
Purdue University  
West Lafayette, IN 47907-1393 (USA)  
Fax: (+1) 765-494-0239  
E-mail: gsimpson@purdue.edu

[b] Prof. R. N. Zare, C. F. Wilson  
Department of Chemistry  
Stanford University  
Stanford, CA 94305-5080 (USA)  
Fax: (+1) 650-723-9262  
E-mail: zare@stanford.edu

[c] Prof. K.-H. Gericke  
Institut für Physikalische und Theoretische Chemie  
der Technischen Universität Braunschweig  
Hans-Sommer-Strasse 10  
38106 Braunschweig (Germany)

 Supporting information for this article is available on the WWW under <http://www.chemphyschem.com> or from the author.

beam. This requirement may not always be consistent with the desired function of the microparticle within a complex device.

Approaches utilizing radio-frequency electric fields have also been demonstrated as viable techniques for noncontact micro-particle manipulation<sup>[6, 8, 19–30]</sup> with unique advantages and limitations. The most well known effect is that of dielectrophoresis (DEP), in which motion is induced in cells and particles with greater or lesser polarizability than the surrounding medium.<sup>[8]</sup> A fundamental requirement for DEP is the presence of an inhomogeneous field (one with a nonzero gradient in the electric field).<sup>[8]</sup> In the simplest scheme for particle manipulation by DEP, translational motion is induced in particles by their attraction or repulsion to the surface of a nonplanar electrode.<sup>[6, 8]</sup> More recently, traveling-wave electric fields have been shown to induce particle motion in a single, well defined direction in a process dubbed traveling-wave dielectrophoresis.<sup>[20–27]</sup> In contrast to optical trapping, particle immobilization by DEP is not trivial but has recently been demonstrated by Schnelle et al.<sup>[28, 29]</sup> using microfabricated octode field cages. Most of these phenomena can be described using a simple, general expression for the time-averaged dielectrophoretic force  $F$  on a sphere, Equation (1),<sup>[8, 30]</sup> in which  $\epsilon_s$  is the dielectric constant of the suspension medium,  $R$  is the particle radius,  $E$  is the amplitude of the driving field, and  $f$  is the Claussius–Mos-sotti factor as given explicitly in the Supporting Information. The factor  $f$  is itself a function of the dielectric properties of both the medium and the particle.

$$\langle F \rangle = 2\pi\epsilon_s R^3 \text{Re}[f] \nabla E^2 \quad (1)$$

The phenomenon of electrorotation (ER), which is the induction of rotation by an external AC electric multipole field, is intimately connected to dielectrophoresis.<sup>[6, 29–34]</sup> In a typical ER measurement, a rotating radio-frequency electric field is applied around three or more electrodes arranged in a multipole. Microfabricated electrode systems can be used to minimize the spacing between electrodes, thereby generating the high fields required for ER studies with moderate applied potentials.<sup>[31, 35–38]</sup> Reichle et al.<sup>[36]</sup> and Schnelle et al.<sup>[28]</sup> have recently employed a system combining microfabricated electrodes with optical tweezers, allowing ER measurements to be recorded on translationally immobilized microparticles and cells. Whereas DEP is dependent on the real part of  $f$ , the time-averaged electrorotational torque  $\langle \tau \rangle$  exerted on a sphere in a multipole field is a function solely of the complex component, Equation (2).<sup>[30]</sup>

$$\langle \tau \rangle = 4\pi\epsilon_s R^3 \text{Im}[f] E^2 \quad (2)$$

Although use of multipole fields to induce ER motion is currently the most common approach, electrorotation can also occur using a purely dipolar electric field, as depicted in Figure 1. In 1960, Teixeira-Pinto et al.<sup>[39]</sup> reported the first observation of cell electrorotation in a dipolar field. Since then, Holzapfel et al.<sup>[40]</sup> and Mahaworasilpa et al.<sup>[33]</sup> have presented theoretical formalisms to treat coupled electrorotation in a dipolar AC field, in which the torque arises through cooperative interactions

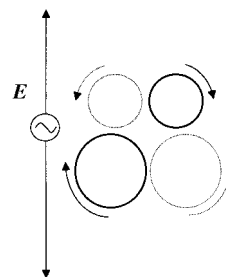


**Figure 1.** Origin of microparticle-coupled electrorotation. Torque is generated through pairwise interactions between the induced dipoles of each spherical particle. Given the nature of the interactions, both particles rotate with the same sense (clockwise, in this case). The dashed lines indicate that fluid flow is induced within the suspension medium from conservation of angular momentum, and are not meant to indicate precise hydrodynamic flow lines.

between the induced dipoles of at least two neighboring particles, as shown in Figure 1. Because these interactions are reciprocal, identical particles experience identical torque.

In this work, the rotational manipulation afforded by coupled electrorotation (CER) was combined with the translational control of optical trapping to controllably induce rotation in individual pairs of microparticles and nanoparticles.

## Microsphere Photopatterning

A practical requirement for all methods used to induce torque in microparticles is a means to characterize and quantify particle rotation. For sufficiently large particles or cells, the rotational frequency as a function of the frequency of the electric field can often be determined by visual inspection. Alternatively, Gimsa and co-workers<sup>[34, 35, 41]</sup> have developed light scattering techniques to quantify particle rotation. Both methods are based on detecting the time-varying change in particle light scattering and/or absorption arising from inherent optical inhomogeneities within the particles. These approaches have the advantage of requiring no additional particle preparation prior to measurement but they suffer from poor reliability in measurements on particles comparable to or smaller than the wavelength of light.

A photopatterning process, depicted in Figure 2, has recently been developed in our laboratory to quantify the rotation of spherical particles.<sup>[42]</sup> Fluorophore-doped polymer microspheres are partially photoaltered and then imaged by laser-induced fluorescence (LIF). For moderate excitation power, this procedure produces inhomogeneous fluorescence profiles within a

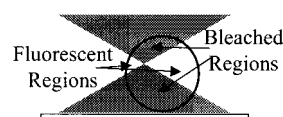


**Figure 2.** Depiction of partial photoalteration of fluorophore-doped microspheres and nanospheres (adapted from ref. [41]). Using an optical trap, a particle was positioned within the focal plane. Brief excitation with an attenuated and focused beam (488 nm for less than 1 s) resulted in photoalteration within the illuminated portions of the sphere. Subsequent fluorescence imaging using wide-field illumination allowed visualization and quantification of rotational motion.

microsphere with no visible changes to the three-dimensional spherical shape. Subsequent analysis of the recorded fluorescence images allows reliable quantification of particle rotation.

## Theory

Mahaworasilpa et al.<sup>[33]</sup> have developed a description of coupled electrorotation for two identical microscopic spheres in close proximity. A generalization of their approach, which describes CER for spheres of different radii with different dielectric properties and different separation distances, is provided in the Supporting Information. Provided a phase lag exists between the external field and the dipole induced in a particle, a dipole will remain after the applied field is removed. Consequently, each sphere can be influenced not only by the external AC field but also by the highly localized dipole field of the neighboring sphere. The resulting localized rotating field produces a torque on each sphere. Two spheres with identical radii and dielectric properties will experience equal torque.<sup>[33]</sup> In the more general case of two dissimilar spheres, considered in detail in the Supporting Information, the torque experienced by one sphere is no longer necessarily equal to that experienced by the other. The interaction between adjacent spheres A and B of radius  $R_A$  and  $R_B$ , respectively, separated by a center-to-center distance  $r$  results in a ratio  $\rho$  of the torques on the spheres given by Equation (3).

$$\rho \equiv \frac{\langle \tau_A \rangle}{\langle \tau_B \rangle} \cong \frac{\text{Im}[f_A] \left( \frac{\text{Im}[f_B] + (R_A/r)^3 \text{Im}[f_A f_B]}{\text{Im}[f_B] + (R_B/r)^3 \text{Im}[f_A f_B]} \right)}{\text{Im}[f_B]} \quad (3)$$

The parameters  $f_A$  and  $f_B$  are the Clausius–Mossotti factors for spheres A and B, respectively. Explicit expressions for  $f_A$  and  $f_B$  are given in the Supporting Information. We find that both spheres of different radii rotate with the same sense, namely both spheres have angular momenta of like sign, in seeming contradiction to the conservation of angular momentum. This behavior can be rationalized by noting that the spheres are suspended in a solvent (which in our study is water). The torque experienced by each sphere is mirrored by a “virtual sphere” within the suspension medium, indicated by the dashed-line spheres in Figure 1. The only requirement imposed by conservation of angular momentum is that the torque experienced by each sphere and its virtual image in the solvent be equal and opposite. This field-induced solvent motion arises from the hydrodynamic flows generated around a rotating spherical object and will be present even if the spheres can rotate but not translate.

The Stokes expression<sup>[6]</sup> for the viscous drag of a rotating sphere, Equation (4), can be used to

$$\langle \tau_A \rangle = -8\pi\eta R^3 \Omega \quad (4)$$

relate the measured rotational period  $\Omega$  with the local viscosity  $\eta$  and the average torque at equilibrium.<sup>[6]</sup> The ratio of the rotational periods for a pair of spheres is then given by Equation (5).

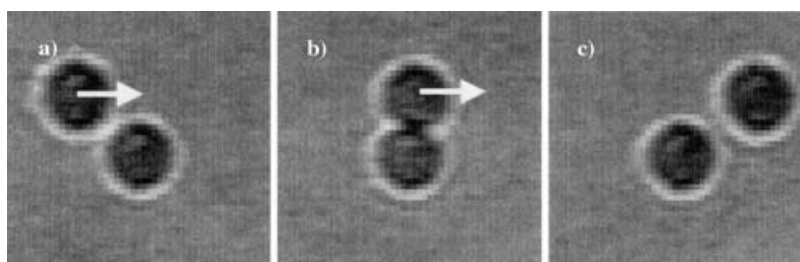
$$\frac{\Omega_A}{\Omega_B} = \rho \left( \frac{R_B}{R_A} \right)^3 \quad (5)$$

As indicated in Equation (5), the ratio of rotation rates for a pair of spheres is intimately linked to the relative sizes, separations, and dielectric properties of the two spheres.

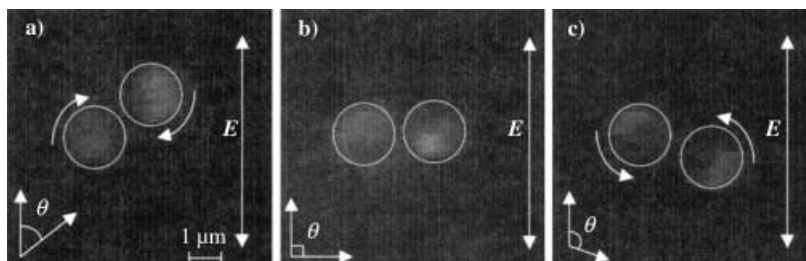
## Results

Figure 3 illustrates microsphere manipulation using the split optical trap. In each image, a 2  $\mu\text{m}$  diameter sphere has been immobilized in each arm of the dual trap. By adjustment of the appropriate mirror, one or both of the two spheres could be controllably repositioned within the focal plane. In the sequence of images shown in Figures 3a–3c, the top sphere was repositioned from left to right.

The relationship between the sense of rotation and the relative position of the particles with respect to the AC field axis was recorded from measurements such as those shown in Figure 4. For particles arranged at an acute angle,  $\theta < 90^\circ$  as shown in Figure 4a, both particles were observed to rotate clockwise by fluorescence imaging. If the particles were aligned either parallel with or perpendicular to the external field, no



**Figure 3.** Sequential images demonstrating simultaneous trapping and independent manipulation of two microscopic particles. The central sphere was maintained at a fixed position within the focal plane, while the upper sphere was repositioned in the directions indicated by the arrows. The particles are 2  $\mu\text{m}$  in diameter.



**Figure 4.** Fluorescence images demonstrating the relationship between the sense of rotation and the sphere orientation within the AC field for 2  $\mu\text{m}$  diameter spheres with an applied potential of 2.5  $\text{kV cm}^{-1}$  and a frequency of 350 kHz. a) Counterclockwise rotation is induced in spheres positioned with  $\theta$  between  $0^\circ$  and  $90^\circ$ ; b) spheres positioned with  $\theta = 0^\circ$ ,  $90^\circ$ , or  $180^\circ$  exhibit no detectable preferential rotation; c) clockwise rotation occurs with  $\theta$  between  $90^\circ$  and  $180^\circ$ . The white outlines specify the geometric edges of the spheres and the bright regions of the images indicate fluorescence.

significant net rotation was observed. The perpendicular case,  $\theta \approx 90^\circ$ , is shown in Figure 4b. Positioning of the particles with an obtuse angle  $\theta$ , as shown in Figure 4c, resulted in counterclockwise rotation of both spheres.

Rates and phases of microsphere rotation were determined from analysis of video footage recorded during fluorescence imaging (an example of such footage can be found in the Supporting Information). Consistent with Equation (2), the rotation rates recorded in this manner scaled quadratically with the applied potential (equivalently, linearly with the field intensity). The fluorescence intensity difference over time for vertical versus horizontal slices through images of each individual particle was fitted to a sine function. This information was used to determine each particle's period and sense of rotation. For clockwise rotation the intensity maximum in the horizontal plane occurs one-quarter of a cycle after the intensity maximum in the vertical plane, suggesting a phase shift  $\delta$  of  $90^\circ$ . Analysis of the data depicted in Figure 4a yielded  $\delta = 104^\circ \pm 8^\circ$  consistent with clockwise rotation, whereas in Figure 4c,  $\delta = -90^\circ \pm 20^\circ$  indicating counterclockwise rotation. The values of these phase shifts quantitatively confirm the assigned directions of rotation indicated by the arrows in Figure 4.

The relationship between the applied field frequency and the particle rotation frequency is exemplified in Figure 5 for a pair of partially photoaltered  $2\ \mu\text{m}$  diameter spheres. To generate each

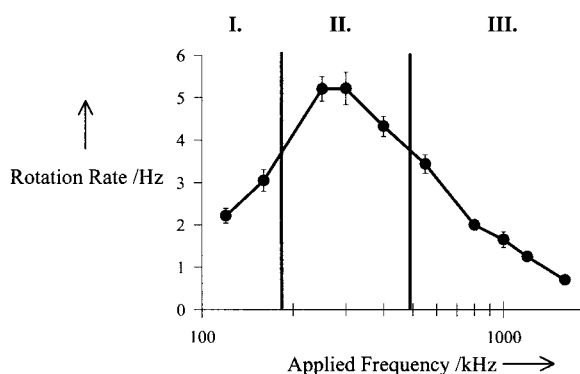


**Figure 5.** Frequency dependence of sphere rotation. Error bars are one standard deviation from between six to eight independent fits of fluorescence intensity difference waveforms (100 points per waveform). In the low-frequency regime (I), the temporal phase shift between the applied field and the dipole field induced in or on the spheres is too small to yield an appreciable local quadrupole field or much rotation. Near the rotation maximum (II), the phase shift is  $\sim 90^\circ$ . In the high-frequency regime (III), the induced dipole only just starts to form when the field is reversed (that is, the phase shift is nearly  $180^\circ$ ).

data point, fluorescence images of the spheres were recorded at each applied frequency, and the rotational periods for the two spheres were averaged. The electrorotation spectrum shown in Figure 5 is qualitatively similar to spectra previously reported for rotation of charged polymer beads in multipole fields.<sup>[31, 43]</sup> Consistent with these earlier studies, the dominant contributions to the sphere polarizabilities at these frequencies and conditions arise from the surface charges of the particles.<sup>[31, 43]</sup>

Figure 6 shows an example of electrorotation for a pair of spheres with dissimilar radii (1.6 and  $2.8\ \mu\text{m}$ ). The LIF images in

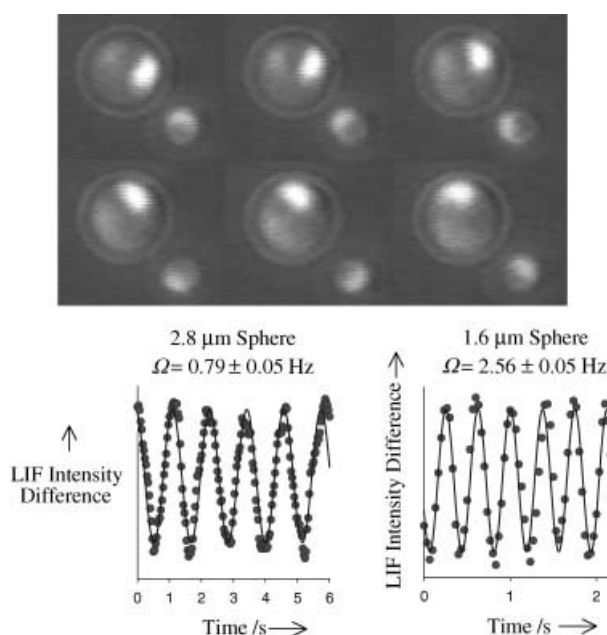
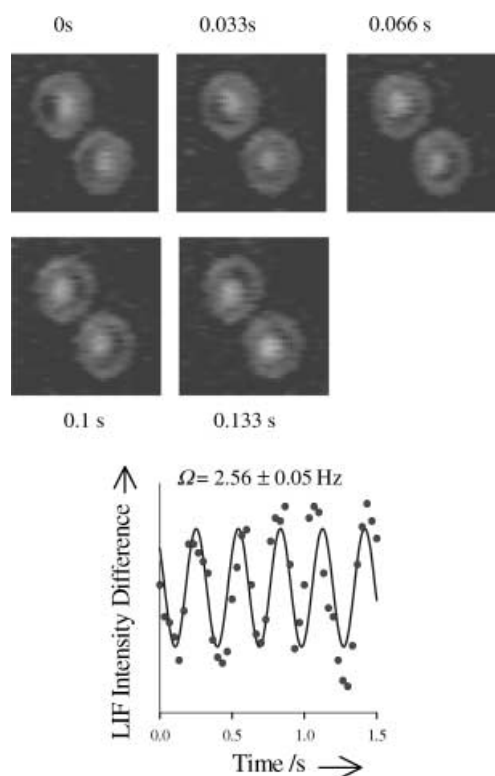


**Figure 6.** Construction of microscopic "antigeers". Each frame contains an LIF image of a partially photoaltered pair of spheres of diameters 2.8 and  $1.6\ \mu\text{m}$ , with sequential images separated by 0.066 s. The bottom two waveforms are fluorescence intensity difference curves (dots), fit to sine waves (solid lines) to extract the rotational period of each sphere. The reported errors in  $\Omega$  are standard deviations of the values from five separate fits, with 200 data points per fit. From the relation of Equation (5),  $\rho = 1.64 \pm 0.05$ .

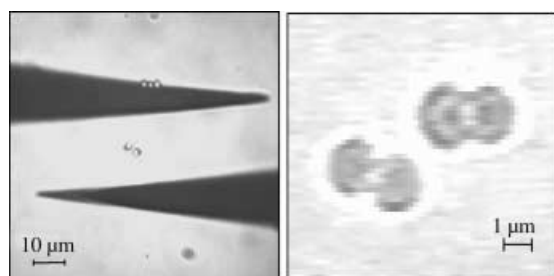
the Figure were separated by time-steps of 0.066 s. The two spheres rotated at different rates as a function of the applied potential and frequency, but the ratio of spin rates remained constant within error (namely, the spheres exhibited registry of motion) with  $\rho_{(2.6/1.6)} = 1.64 \pm 0.05$ . For an applied peak-to-peak potential of  $3.4\ \text{kV cm}^{-1}$ , fits of the fluorescence intensity difference across each bead yielded a rotational period of  $9.19 \pm 0.08\ \text{Hz}$  ( $N=4$ ) for the  $2.8\ \mu\text{m}$  sphere as shown in Figure 6. At this higher applied potential, the  $1.6\ \mu\text{m}$  sphere was rotating too quickly for the motion to be resolved with video rate imaging (30 Hz). The registry of motion observed at lower potentials allowed a rotation rate of  $30 \pm 1\ \text{Hz}$  ( $1800 \pm 60\ \text{rpm}$ ) to be inferred for the  $1.6\ \mu\text{m}$  sphere at an applied potential of 3.4 V. For the electrode spacing employed, higher potentials resulted in ejection of the spheres from the region between the electrodes.

Figure 7 presents fluorescence images for a pair of 750 nm spheres along with fits to the intensity differences across each bead with time. Adjacent images were acquired at a video rate of 30 Hz. Analysis yielded spin rates of  $150 \pm 90\ \text{rpm}$ .

Figure 8 contains bright field and fluorescence images of a pair of optically trapped fused microspheres, which we refer to as dimers, made to rotate in an AC field. A small fraction of microsphere dimers was inherently present in the sphere solutions prior to use, presumably formed either during the manufacturing process itself or during the dilution/centrifugation treatments typically performed prior to use. Upon immobilization in an optical trap, the dimers oriented with their long axes parallel to the propagation direction of the optical trap



**Figure 7.** Sequence of fluorescence images for a pair of 750 nm diameter rotating spheres, along with a representative sine fit of the fluorescence difference data. The combined results from 16 fits yielded a mean rotation rate of  $150 \pm 90$  rpm.



**Figure 8.** Bright-field images of a pair of microsphere dimers. Left: An expanded view indicating the most common arrangement of the microelectrodes used to induce rotation. Both dimers in the left panel are optically trapped and aligned with the dimer axis approximately parallel with the beam axis. Right: Bright field images of the dimers immediately after being released from the trap. Fits of the intensity difference yielded a rotation rate of  $\Omega = 2.42 \pm 0.09$  Hz ( $N = 10$  fits, 100 points per fit).

beam and perpendicular to the focal plane. This preferred orientation of rodlike particles is consistent with a greater trapping force perpendicular, versus parallel, to the trap beam axis.<sup>[3]</sup> The only dimer rotational motion observed upon partial photoalteration followed by LIF imaging was about the dimer axes.

In order to exploit the registry of sphere rotation to probe the dielectric properties of immobile objects, a sealed micropipette served as a third particle in a coupled electrorotation study, depicted in Figure 9. When the micropipette tip was positioned adjacent to a pair of optically trapped 1.6  $\mu\text{m}$  diameter micro-

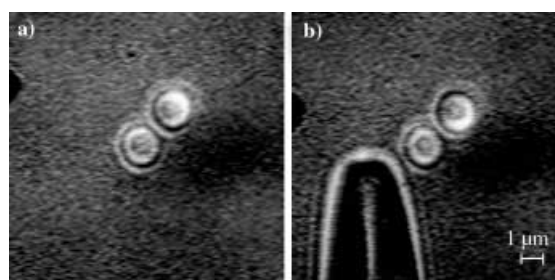


**Figure 9.** Coupled electrorotation in multiple objects. a) Fluorescence images of a pair of 1.6  $\mu\text{m}$  diameter photopatterned spheres rotating in an AC field; b) the same rotating spheres after a sealed glass pipette tip is introduced. The ratio of rotation rates for the sphere-pair (that of the bottom-left divided by that of the top-right) changed from  $1.0 \pm 0.1$  for the isolated sphere-pair to  $1.28 \pm 0.05$  upon positioning of the glass tip next to the lower left sphere.

spheres, the registry of motion between the two spheres changed. Specifically,  $\Omega_1/\Omega_2$  changed from  $1.0 \pm 0.1$  for the isolated pair ( $\rho$  should equal unity for identical spheres) to  $\Omega_1/\Omega_2 = 1.28 \pm 0.05$  in the presence of the rounded glass tip (the subscript 1 denotes the sphere closest to the rounded tip). In both cases,  $\rho$  was determined from nine measurements, with the rotation rate of each sphere in each measurement obtained from fits of  $\sim 100$  data points. Given the cubic dependence of the rotation rate on the interparticle distance, interactions between the micropipette tip and the far sphere may be assumed negligible compared with the interactions between the tip and the nearest sphere. If it is assumed that the dielectric properties of the spheres and pipette tip are similar, the net torque exerted on the pipette tip will be comparable to the change in torque induced in sphere 1 upon introduction of the pipette. The Stokes–Einstein relation  $|\langle \Delta\tau \rangle| = 8\pi\eta R_{\text{sphere}}^3 \Delta\Omega$  expresses the change in the average torque  $\langle \Delta\tau \rangle$  in terms of the viscosity  $\eta$  and the change in rotational frequency  $\Delta\Omega$  of sphere 1 upon interaction with the pipette tip. In the experiment depicted in Figure 9,  $\Delta\Omega = 0.4 \pm 0.2$  Hz, yielding a measured  $\langle \Delta\tau \rangle$  of  $4 \pm 2 \times 10^{-20}$  N m, or 40 zN m, of torque.

## Discussion

The potential utility of coupled electrorotation for particle manipulation and device development can be assessed by considering several figures of merit, such as the range of rotation rates possible, the duration of rotation, the range in the size and shape of particles that may be manipulated, the information content that may be obtained, and the instrumentation requirements to induce rotation.

As established in Figure 6, sustained rotation rates of  $1800 \pm 60$  rpm for a 1.6  $\mu\text{m}$  diameter sphere have been recorded from CER measurements. In previous studies by Chen and Berg,<sup>[44]</sup> electrorotation rates in excess of 350 Hz (21 000 rpm) have been achieved for *E. coli* in a multipole field. Considering that the rotation rate scales inversely with the radius cubed, halving the particle sizes in CER measurements should yield an increase in the possible rotation rate of almost an order of magnitude. The quadratic dependence of the rotation rate on the applied potential suggests that rotation rates comparable to those

achieved by Chen and Berg<sup>[44]</sup> should be obtainable using nanoscopic particles.

The instability observed at high rotation rates has several possible origins. Dielectrophoretic attraction to or repulsion from the curved microelectrode surfaces could result in ejection of the particles from the trap. In this case, stability could be increased by optimizing the applied AC frequency to minimize the dielectrophoretic forces. Additionally, electroosmotic flow has been shown to contribute significantly to electrorotation in low-frequency quadrupole field studies using electrolyte solutions.<sup>[45]</sup> Alternatively, Grzybowski et al. have demonstrated that hydrodynamic flows surrounding millimeter-scale magnetic disks rotating with the same sense at rotation rates between several hundred and a thousand rpm lead to an effective repulsion between adjacent disks.<sup>[46, 47]</sup> For the high rotation rates attained by the sphere pair shown in Figure 6, the instability observed may have resulted from a similar effect but on microscopic length scales. If the observed instability was largely hydrodynamic in origin, then the possibility exists to use CER to directly probe localized hydrodynamic phenomena.

Theoretically, particle rotation can be sustained indefinitely provided the properties of the suspension medium remain constant. In our investigations, the rotation of a single particle pair was maintained for nearly four hours. Use of a closed system to reduce evaporation and exposure to airborne contaminants should significantly extend the duration with which a single particle or a set of particles can be made to rotate.

The range of particle sizes that may be rotated using a given technique has obvious ramifications on the general applicability of the approach. For an instrument utilizing optical tweezers similar to those used in these investigations, the particle size range is determined by the ease of optical trapping. An upper bound for optical trapping in solution is approximately 100  $\mu\text{m}$ .<sup>[4]</sup> Although single molecules in solution have shown evidence of being optically trapped optically,<sup>[48]</sup> a practical lower bound for selecting and trapping a single particle in aqueous solution is about 500 nm. Optical trapping of isolated particles much smaller than 500 nm in diameter is not limited by the particle instability within the trap (in fact,  $\sim 50$  nm is a practical lower bound for optical trapping of dielectric particles in solution<sup>[4]</sup>) but rather by its rapid Brownian motion outside the trapping region complicating the initial immobilization.

For charged polymer particles in aqueous solutions, studies by Maier<sup>[43]</sup> suggest that the radio-frequency particle polarizability is a function largely of the surface charge rather than the three-dimensional geometric structure. In contrast to many of the purely optical manipulation methods, the torque induced by CER at these applied frequencies is not directly dependent on the three-dimensional particle structure, consistent with the dimer studies shown in Figure 8 and the third-body investigations in Figure 9. These results demonstrate that torque could be induced in more complicated particle architectures using CER methods. This flexibility may be of particular importance in fabrications of microelectromechanical devices, in which the functioning structural mechanism might not be compatible with inherent shape requirements for inducing rotation.

The information content available in coupled electrorotation measurements of microscopic particles is particularly interesting for a pair of dissimilar particles. In contrast to both traditional gears and initial intuition, the magnitude of the torque on one sphere in the pair does not necessarily equal that on the other. In fact, Equation (3) predicts that the torque on each will be equal only if  $\rho$  is equal to unity, in good agreement with experimental observations (see Figure 7). For identical spheres of the same size,  $\rho$  will invariably equal unity and both the torques and rotation rates of the two spheres should be equal, a trend confirmed experimentally in measurements such as those shown in Figures 4 and 7. For dissimilar spheres, such as those shown in Figure 6,  $\rho$  is a function of both the polarizability of the solvent and the difference in polarizability between the two spheres. It is reasonable to suggest that the difference in torque experienced by the 1.6 and 2.8  $\mu\text{m}$  spheres depicted in Figure 6 is related to surface functionality (the 1.6  $\mu\text{m}$  spheres had carboxylate-terminated surfaces while the 2.8  $\mu\text{m}$  spheres did not). The expression for  $\rho$  given in Equation (3) and the experiments described by Figure 6 suggests experiments can be designed to "tune" the registry of motion by manipulating the dielectric properties of the suspension medium. Alternatively, experimentally observed changes in  $\rho$  may be correlated with changes in the surface properties of the rotating particles, providing a means for localized chemical sensing.

As described in Figure 9, the change in the ratio of rotation rates for a pair of spheres can also be used to estimate the torque exerted on a stationary object. Torque measurements in the zeptoNewton-meter range were easily generated and quantified. These three-particle results demonstrate that CER measurements are not limited to studies of only two particles. With the continuing development of techniques to independently position multiple particles using a single optical trapping beam,<sup>[49, 50]</sup> it is not difficult to envision microscopic "antigear" arrays of particles rotating in concert.

Lastly, the instrumentation required for inducing particle rotation is both straightforward and highly compatible with incorporation into micromechanical device platforms. In the simplest instances, all that is needed to induce torque in particles is a pair of microelectrodes, a source of a radio-frequency electrical potential, and a means to controllably position microparticles. For small gaps between the electrodes ( $\sim 5$  to 20  $\mu\text{m}$ ), the fields necessary to induce rotation can be generated using widely available low-voltage sources such as the one employed in these studies.

## Conclusions

Coupled electrorotation was demonstrated as a viable means to controllably induce rotation in microscopic and nanoscopic particles. Particles of different sizes exhibited registry of motion, with the ratio of the torque exerted on each sphere being a function of the relative particle polarizability. Exploiting this registry of motion, rotation rates as high as 1800 rpm were achieved for moderate applied potentials. Rotation has been induced in particles as small as 750 nm in diameter and in fused sphere dimers. Changes in the relative rotation rates for a pair of

particles were used to estimate the CER torque exerted on a stationary object.

Advantages of CER for both sensing applications and incorporation into microelectromechanical devices include a) rotation can be induced with a simple electrical system and moderate applied potentials, b) rotation is a function of polarizability, such that essentially any carefully engineered nanostructure can be made to spin, c) multiple particles can be made to rotate in registry, with the potential for generation of complex multicomponent systems where the components rotate in concert, and d) theory predicts that the registry of motion may be "tuned" by changing the dielectric properties of the particle and/or solvent to affect  $\rho$  in a controlled manner. Continuing theoretical and experimental studies are in progress to extend the capabilities and applications of CER measurements, including investigations using microfabricated electrodes.

## Experimental Section

Particle rotation measurements were acquired using a Nikon Diaphot inverted microscope, with images collected by a silicon intensified target (SIT, Hamamatsu C2400-08) camera and recorded onto videotape. Figure 10 shows a schematic of the instrument. The approach used to generate a dual optical trap is similar to that described previously by Visscher et al.<sup>[45]</sup> In brief, light from a 985 nm master oscillator power (diode) laser (MOPA; 1 W, SDL Model 5762-A6) for optical trapping was introduced into a 1:1 telescope to allow alignment of the trapped particles within the visible focal plane. Next the trap laser beam was split into its two polarization components using a beam-splitting cube, then recombined at a second beam-splitting cube such that the two beams were nearly parallel as they entered the back of the microscope objective (Nikon, 1.4 N.A.). Adjustment of a mirror allowed independent manipulation of one particle with respect to the other within the focal plane. A dichroic mirror allowed the introduction of both the optical trapping beams as well as the 488 nm excitation beam from an argon ion laser (SpectraPhysics Stabilite 2017) into the microscope.

Prior to each measurement, a new glass coverslip was placed over the oil-immersion  $100\times$  objective, and a droplet of spheres suspended in water was placed on the slide. Fluoresbrite yellow-green microspheres (0.75, 1.6, and  $2.8\ \mu\text{m}$ , Polysciences, Inc) were used as purchased; the 0.75 and  $1.6\ \mu\text{m}$  spheres had carboxylate-terminated surfaces while the  $2.8\ \mu\text{m}$  spheres were not prepared with any specific surface functionality. Yellow-green carboxylated FluoSpheres ( $2\ \mu\text{m}$ , Molecular Probes) were also used as purchased. Commercial scanning tunneling microscope tips (PtIr Nanotips, Digital Instruments) were used as microelectrodes, and positioned within the droplet using micromanipulators. Each measurement proceeded as follows: a) one particle was immobilized in the primary optical trap and positioned at the focal point of the excitation laser; b) the particle was partially photoaltered with focused 488 nm light between 0.1 and 3 s depending on the bead size; c) this particle was transferred to the secondary trap and relocated; d) a second particle was immobilized in the primary trap and photoaltered; and e) LIF measurements were acquired with wide-field 488 nm excitation by passing the excitation beam through a spinning disk diffuser. The bleaching time for beads was selected to be less than the time required for the microsphere to undergo rotational diffusion by more than a few degrees.

The AC output from a function generator (Stanford Research Systems) was coupled directly to the microelectrodes, with frequencies of 400–700 kHz to optimize sphere rotation and to minimize dielectrophoretic attraction/repulsion. Most measurements were recorded for peak-to-peak potentials of 1.5 V or less. The distance between microelectrodes was generally between  $\sim 10$ – $20\ \mu\text{m}$ . Most measurements were recorded with the electrodes positioned in a side-to-side configuration (shown in Figure 8) as opposed to tip-to-tip. Consistent with previous findings,<sup>[51–53]</sup> isolated, single spheres did not rotate significantly under these conditions, confirming that fluid flow is unimportant in the present experiments. It should be mentioned, however, that in an electrolyte solution the main cause of particle rotation can be electroosmotic flow, as shown by Grosse and Shilov.<sup>[51]</sup>

Particle rotation rates were determined by digitization of the LIF video images. In a single image, the difference in average fluorescence intensity between the left and right halves of a given particle was calculated. Fluorescence intensity difference waveforms were generated by repeating this analysis for a stack of 100 or 200 images, and the rotational period determined from fits of the waveforms to sine waves. Rotation rates did not change significantly over the timescales used for data acquisition (a few minutes or less). Evaporation of the droplet resulted in noticeable changes in the rotation rates for longer times (between  $\sim 15$  min to well over 3 h, depending on the droplet size).

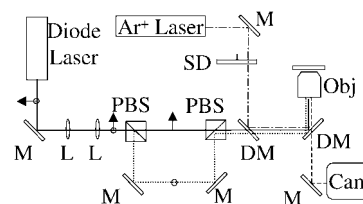


**Figure 10.** Instrumentation schematic. The optical trapping beam from a diode laser (985 nm, linearly polarized at  $\sim 45^\circ$  indicated by the circle and the arrow) was directed off a mirror (M) through a pair of lenses (L) acting as a 1:1 telescope to a polarizing beam-splitting cube (PBS). The reflected component of the beam was recombined at a second PBC, introduced into the microscope through one dichroic mirror (DM) and into the objective (Obj) with another. Provided the two recombined trap beams were not exactly collinear, each polarization component focused to a different location within the focal plane. Adjustment of the final lens of the telescope allowed alignment of the upper arm of the trap to be nearly coincident with the focal point of the beam causing photoalteration. By adjusting the final mirror in the lower arm of the dual trap, the position of one trapped particle with respect to the other was independently manipulated. Light from the 488 nm argon ion laser was used to perform partial photoalteration as well as fluorescence imaging. To photoalter, the attenuated beam was reflected off two dichroic mirrors through a  $100\times$  microscope objective to the trapped particle with timing controlled by a shutter. Wide-field fluorescence excitation was accomplished by introducing a frosted spinning disk (SD) prior to the first dichroic mirror. The fluorescent emission passed through a dichroic mirror and appropriate optical filters before being detected by an SIT camera (Cam).

This work was supported by the U.S. National Institute on Drug Abuse. G.J.S. thanks Pfizer and the Life Sciences Research Foundation for a postdoctoral fellowship. C.F.W. expresses his thanks for a DuPont Pharmaceutical Graduate Fellowship.

- [1] M. Koch, A. Evans, A. Brunnschweiler, *Microfluidic Technology and Applications*, Research Studies Press, Baldock, 2000.
- [2] N. Maluf, *An Introduction to Microelectromechanical Systems Engineering*, Artech House, Boston, MA, 2000.

- [3] A. Ashkin, *Biophys. J.* **1992**, *61*, 569.
- [4] K. Svaboda, S. M. Block, *Annu. Rev. Biophys. Biomol. Struct.* **1994**, *23*, 247.
- [5] S. M. Block, *Noninvasive Techniques in Cell Biology* (Eds.: J. K. Foskett, S. Grinstein), John Wiley and Sons, New York, NY, **1990**, Chap. 15.
- [6] T. B. Jones, *Electromechanics of Particles*, Cambridge University Press, New York, NY, **1996**.
- [7] G. V. G. Seaman, D. E. Brooks, *Electrokinetic Separations Methods*, Elsevier, New York, NY, **1979**, Chap. 6.
- [8] H. A. Pohl, *Dielectrophoresis*, Cambridge University Press, New York, NY, **1978**.
- [9] R. Pethig, Y. Huang, *Bioelectrochemistry of Cells and Tissues*, 2nd ed., Birkhäuser Verlag, Boston, MA, **1995**, Chap. 6.
- [10] P. Galajda, P. Ormos, *Appl. Phys. Lett.* **2001**, *78*, 249.
- [11] E. Higurashi, R. Sawada, T. Ito, *Appl. Phys. Lett.* **1998**, *72*, 2951.
- [12] E. Higurashi, H. Ukiwa, H. Tanaka, O. Ohguchi, *Appl. Phys. Lett.* **1994**, *64*, 2209.
- [13] A. Yamamoto, I. Yamaguchi, *Jpn. J. Appl. Phys.* **1994**, *34*, 3104.
- [14] M. E. J. Friese, T. A. Nieminen, N. R. Heckenberg, H. Rubinsztein-Dunlop, *Nature* **1998**, *394*, 348.
- [15] M. E. J. Friese, H. Rubinsztein-Dunlop, J. Gold, P. Hagberg, D. Hanstorp, *Appl. Phys. Lett.* **2001**, *78*, 547.
- [16] N. B. Simpson, K. Dholakia, L. Allen, M. J. Padgett, *Opt. Lett.* **1997**, *22*, 52.
- [17] N. B. Simpson, L. Allen, M. J. Padgett, *J. Mod. Opt.* **1996**, *43*, 2485.
- [18] L. Paterson, M. P. MacDonald, J. Arlt, W. Sibbett, P. E. Bryant, K. Dholakia, *Science* **2001**, *292*, 912.
- [19] R. Hagadorn, G. Fuhr, T. Müller, J. Gimsa, *Electrophoresis*, **1992**, *13*, 49.
- [20] M. P. Hughes, *Nanotechnology* **2000**, *11*, 124.
- [21] B. Malyan, W. Balachandran, *J. Electrostat.* **2001**, *51–52*, 15.
- [22] N. G. Green, A. Ramos, H. Morgan, *J. Phys. D: Appl. Phys.* **2000**, *33*, 632.
- [23] L. Cui, H. Morgan, *J. Micromech. Microeng.* **2000**, *10*, 72.
- [24] M. P. Hughes, R. Pethig, X.-B. Wang, *J. Phys. D: Appl. Phys.* **1995**, *28*, 474.
- [25] A. D. Goater, J. P. H. Burt, R. Pethig, *J. Phys. D: Appl. Phys.* **1997**, *30*, L65.
- [26] X.-B. Wang, Y. Huang, F. F. Becker, P. R. C. Gascoyne, *J. Phys. D: Appl. Phys.* **1994**, *27*, 1571.
- [27] N. G. Green, M. P. Hughes, W. Monaghan, H. Morgan, *Microelectron. Eng.* **1997**, *35*, 421.
- [28] T. Schnelle, T. Müller, G. Gradl, S. G. Shirley, G. Fuhr, *Electrophoresis* **2000**, *21*, 66.
- [29] T. Schnelle, T. Müller, C. Reichle, G. Fuhr, *Appl. Phys. B: Lasers Opt.* **2000**, *70*, 267.
- [30] J. C. Baygents, *Colloids Surf. A* **1994**, *92*, 67.
- [31] W. M. Arnold, U. Zimmerman, *J. Electrostat.* **1988**, *21*, 151.
- [32] H. P. Schwan, *Ferroelectrics* **1988**, *86*, 205.
- [33] T. L. Mahaworasilpa, H. G. L. Coster, E. P. George, *Biochim. Biophys. Acta* **1996**, *1281*, 5.
- [34] J. Gimsa, *Colloids Surf. A* **1999**, *149*, 451.
- [35] B. Prüger, P. Eppmann, J. Gimsa, *Colloids Surf. A* **1998**, *136*, 199.
- [36] C. Reichle, T. Schnelle, T. Müller, T. Leya, G. Fuhr, *Biochim. Biophys. Acta* **2000**, *1459*, 218.
- [37] T. Schnelle, R. Hagedorn, G. Fuhr, S. Fielder, T. Müller, *Biochim. Biophys. Acta*, **1993**, *1157*, 127.
- [38] G. Fuhr, H. Glassner, T. Müller, T. Schnelle, *Biochim. Biophys. Acta* **1994**, *1201*, 353.
- [39] A. A. Teixeira-Pinto, L. L. Nejelski, Jr., J. L. Culter, J. H. Heller, *Exp. Cell Res.* **1960**, *20*, 548.
- [40] C. Holzäpfel, J. Vienken, U. Zimmermann, *J. Membr. Biol.* **1982**, *67*, 13.
- [41] J. Gimsa, B. Prüger, P. Eppmann, E. Donath, *Colloids Surf. A* **1995**, *98*, 243.
- [42] G. J. Simpson, T. Wholand, R. N. Zare, *Nano Lett.*, **2002**, *2*, 207.
- [43] H. Maier, *Biophys. J.* **1997**, *73*, 1617.
- [44] X. Chen, H. C. Berg, *Biophys. J.* **2000**, *78*, 1036.
- [45] K. Visscher, S. P. Gross, S. M. Block, *IEEE J. Quantum Electron.* **1996**, *2*, 1066.
- [46] B. Z. Grzybowski, H. A. Stone, G. M. Whitesides, *Nature* **2000**, *405*, 1033.
- [47] B. Z. Grzybowski, X. Jiang, H. A. Stone, G. M. Whitesides, *Phys. Rev. E* **2001**, *64*, 11603.
- [48] D. T. Chiu, R. N. Zare, *J. Am. Chem. Soc.* **1996**, *118*, 6512.
- [49] K. Visscher, S. P. Gross, S. M. Block, *IEEE J. Quantum Electron.* **1996**, *2*, 1066.
- [50] E. Fällman, O. Axner, *Appl. Opt.* **1997**, *36*, 2107.
- [51] C. Grosse, V. N. Shilov, *Colloids Surf. A* **1998**, *140*, 199.
- [52] C. Grosse, V. N. Shilov, *J. Phys. Chem.* **1996**, *100*, 1771.
- [53] B. Neu, R. Georgieva, H. Bäuml, V. N. Shilov, E. Knippel, E. Donath, *Colloids Surf. A* **1998**, *140*, 325.

---

Received: September 24, 2001 [F314]

Revised: February 15, 2002